A GFP-based genetic screen reveals mutations that disrupt the architecture of the zebrafish retinotectal projection

Tong Xiao, Tobias Roeser, Wendy Staub and Herwig Baier*

Department of Physiology, University of California, San Francisco, Programs in Neuroscience, Genetics, Human Genetics, and Developmental Biology, 1550 4th Street, San Francisco, CA 94158-2722, USA
*Author for correspondence (e-mail: hbaier@itsa.ucsf.edu)

Accepted 14 April 2005

Development 132, 2955-2967
Published by The Company of Biologists 2005
doi:10.1242/dev.01861

Summary

The retinotectal projection is a premier model system for the investigation of molecular mechanisms that underlie axon pathfinding and map formation. Other important features, such as the laminar targeting of retinal axons, the control of axon fasciculation and the intrinsic organization of the tectal neuropil, have been less accessible to investigation. In order to visualize these processes in vivo, we generated a transgenic zebrafish line expressing membrane-targeted GFP under control of the *brn3c* promoter/enhancer. The GFP reporter labels a distinct subset of retinal ganglion cells (RGCs), which project mainly into one of the four retinorecipient layers of the tectum and into a small subset of the extratectal arborization fields. In this transgenic line, we carried out an ENU-mutagenesis screen by scoring live zebrafish larvae for anatomical phenotypes. Thirteen recessive mutations in 12 genes were discovered. In one mutant, *ddl*, the majority of RGCs fail to differentiate. Three of the mutations, *vrt*, *late* and *tard*, delay the orderly ingrowth of retinal axons into the tectum. Two alleles of *drg* disrupt the layer-specific targeting of retinal axons. Three genes, *fuzz*, *beyo* and *brek*, are required for confinement of the tectal neuropil. Fasciculation within the optic tract and adhesion within the tectal neuropil are regulated by *vrt*, *coma*, *bluk*, *clew* and *blin*. The mutated genes are predicted to encode molecules essential for building the intricate neural architecture of the visual system.

Key words: Retinal ganglion cell, Tectum, Transgenic, Mutant, Axon guidance, *brn3c*, *pou4f3*, Zebrafish

Introduction

Work over the past decade has increased our understanding of the mechanisms involved in specifying neuronal connections. Long-range axon guidance in the vertebrate CNS is mediated by a handful of families of axon guidance molecules, notably ephrins, semaphorins, Slit proteins and netrins (Dickson, 2002). Moreover, molecules involved in close-range synaptic recognition have been identified, including cadherins and immunoglobulin superfamily molecules (Biederer et al., 2002; Serafini, 1999; Yamagata et al., 2002). The visual system, particularly the projection from the retina to the optic tectum, has long served as a discovery vehicle for new mechanisms, as well as a testing ground for candidate factors (Dingwell et al., 2000; McLaughlin et al., 2003). For example, netrin 1 is required to guide retinal axons into the optic nerve (Deiner et al., 1997), while Slit proteins channel RGC axons through the optic tract (Fricke et al., 2001). Moreover, ephrin A proteins direct the mapping of temporal axons onto the anterior tectum (Drescher et al., 1997; Flanagan and Vanderhaeghen, 1998), while semaphorin 3D (Liu et al., 2004) and EphB proteins (Hindges et al., 2002; Mann et al., 2002) carry out the equivalent function along the dorsoventral axis.

Most of the molecular players listed above have been identified through biochemical purification or by candidate gene approaches. A forward-genetic screen provides an alternative strategy to reveal novel genes (or new functions for known genes) in an unbiased manner. A previous anatomical screen for retinotectal projection defects in zebrafish used fluorescent lipophilic dyes to trace RGC axons as they navigated to the tectum. Two carbocyanine dyes, DiI and DiO, were injected at different locations into the retina of larval zebrafish, thus labeling separate subpopulations of RGCs terminating in topographically distinct regions of the tectum (Baier et al., 1996; Karlstrom et al., 1996; Trowe et al., 1996). This large-scale screen uncovered 114 mutations, in about 35 genes, disrupting either the pathfinding of axons from the eye to the tectum or the retinotopic map. Although some of the more specific mutations, such as *gna*, *woe* and *nev*, still await molecular identification, most of the genes have now been cloned (Culverwell and Karlstrom, 2002). Unsurprisingly, retinotectal pathfinding was found to depend on proper brain patterning (Hedgehog signaling, *syu*, *igu*, *con*, *dtr*, *uml* and *yot*; Nodal signaling, *cyc*; homeodomain transcription factors, *noi*) and on components of the extracellular matrix (*bal*, *gpy* and *sly*). A small minority of mutations was found to disrupt specific signaling pathways within the retinal growth cones, such as those mediated by Slit/Robo (*ast*) (Fricke et al., 2001), heparan sulfate proteoglycans (*box* and *dak*) (Lee et al., 2004) or PAM/highwire (*esr*) (D'Souza et al., 2005).

Although productive with regard to isolating retinotectal mutants, this first screen was laborious and intrinsically limited to finding only a subset of interesting phenotypes. Important

organizing principles of retinotectal connectivity, such as neuropil assembly and laminar targeting of RGC axons could not be investigated with the screening method employed. As a consequence, the factors that assemble the characteristic architecture of optic tract and tectum and coordinate the development of the visual system are still elusive. We expect that disruption of some of these factors may lead to relatively subtle anatomical alterations, whose detection and analysis require sensitive methods. As structural changes of the CNS will ultimately influence its function, mutations in the human homologs of these genes might turn out to be responsible for neurological and psychiatric diseases.

We have developed a screening strategy aimed at discovering specific disruptions of retinotectal architecture. Enhancer sequences from the zebrafish *brn3c* gene were used to drive membrane-targeted GFP in a distinct subset of RGCs. GFP-based forward-genetic screens have been employed extensively in *Drosophila* and *C. elegans*, and more recently in zebrafish (Lawson et al., 2003). The use of a genetically encoded label overcomes the limitations of dye injections. First, the screening assay is rapid, because fish do not need to be aldehyde fixed and injected. Second, the labeling is robust and reproducible among fish, thus allowing the detection of even subtle abnormalities. Finally, the GFP label allows the observation of the same fish at multiple stages of development. We tested the suitability of the *Brn3c:mGFP* transgenic line in a screen of 233 ENU-mutagenized F2 families. Our relatively small-scale effort (three investigators, 1 year) detected 13 novel phenotypes, including ones in which the retinotectal projection is delayed or disorganized. These new mutants should add to a cellular and molecular understanding of the processes that generate precise neuronal connections in the visual system and other parts of the nervous system.

Materials and methods

Fish breeding

Zebrafish of the TL strain were raised and bred at 28.5°C on a 14 h light/10 h dark cycle. Embryos were produced by natural crosses and staged by hours or days post fertilization (hpf or dpf).

Cloning of zebrafish *brn3b* and *brn3c*

A 168 bp *brn3b* fragment was cloned from zebrafish cDNA by degenerate PCR. Further parts of the sequence were obtained using degenerate primers targeted to conserved regions at the 5′ and 3′ ends of the *brn3b* sequence. At least two clones from independent PCR reactions were sequenced. Primers to the resulting consensus sequence of these fragments were used to identify genomic PAC clones in a pooled PAC library available from RZPD (Berlin, Germany) (Amemiya and Zon, 1999). Three clones contained *brn3b*. The remaining *brn3b* sequence was obtained by direct sequencing from PAC clones BUSMP706A1597Q2 and BUSMP706N19174Q2 from RZPD. The GenBank Accession Number for *brn3b* is AF395831.

Zebrafish full-length *brn3c* was identified as for *brn3b*, except that primers for nested PCR were designed based on a partial cDNA sequence published previously (Sampath and Stuart, 1996). The GenBank Accession Numbers for full-length *brn3c* and its first intron are AY995217 and AY995218. The forward primers were 5′-GGC AAT ATA TTC AGC GGC TTT G-3′ and 5′-GCT AAA CTC CTC GTA TTG TTA C-3′. The reverse primers were 5′-GTA TCT TCA GGT TGG CGA GAG-3′ and 5′-GGA GGA AAT GTG GTC GAG TAG-3′. Three positive PAC clones were identified.

Construction of the *Brn3c:mGFP* transgenic vector

The *brn3c*-containing PACs were characterized by restriction digests and Southern hybridization. A 7.5 kb *Bsp*EI fragment was identified that contained part of the *brn3c*-coding region and 6 kb of upstream sequence. It was subcloned from PAC clone BUSMP706K02247Q2 and partially sequenced. The PAC sequences, together with a 5′ RACE product, yielded the remaining parts of the zebrafish *brn3c* sequence and identified the putative translation start. The 6 kb promoter fragment was cloned into pG1, a GFP expression vector (kindly provided by C.-B. Chien, MPI Tübingen). For membrane targeting, the sequence encoding the first 20 amino acids of zebrafish GAP43 (Kay et al., 2004) was generated from two overlapping oligonucleotides, which also contained a *Xenopus* β-globin ribosomal binding site. The sequences were 5′-G GAA TTC CAC GAA ACC ATG CTG TGC TGC ATC AGA AGA ACT AAA CCG GTT GAG AAG-3′ and 5′-TCC CCC GGG CTG CAG CTG ATC GGA CTC TTC ATT CTT CTC AAC CGG TTT AGT-3′. The oligonucleotides were fused, filled in with Klenow Polymerase, and cloned into the *Pst*I and *Eco*RI site of the *brn3c* promoter. The resulting pTR56 vector was used to generate transgenic zebrafish (see below).

Generation of transgenic fish

The insert from vector pTR56 was excised by digestion with *Not*I and separated from the vector backbone by agarose gel electrophoresis. The DNA was extracted and eluted in 10 mM triethanolamine (Tris, pH 7.5). Prior to injection, the DNA was diluted in water containing 0.05% Phenol Red (Sigma) to 10-20 ng/μl. Injected embryos were raised to sexual maturity and crossed to identify founder fish. The embryos from these crosses were scored for their GFP expression and raised. This effort led to the production of several stable lines, one of which was used in this study. The official designation of this line is *TG(Brn3c:GAP43-GFP)*^{s356t} (http://www.zfin.org).

Mutagenesis

To efficiently induce random point mutations in the zebrafish genome, we followed published protocols (van Eeden et al., 1999). Briefly, adult male TL fish were treated three to five times at weekly intervals with ENU (3.0 mM, 1 hour). Four weeks after the last treatment, they were outcrossed to produce up to 200 F1 fish per male. These F1 fish were crossed to *Brn3c:mGFP*^{s356t} carriers to generate F2 families. Six or more pairs of random crosses were set up between siblings for each F2 family. In total, 233 F2 families were screened.

Screening assay

Embryos (3 dpf) and larvae (6 dpf) were embedded in 2.5% methylcellulose in E3 medium (5 mM NaCl, 0.17 mM KCl, 0.33 mM $CaCl_2$, 33 mM $MgSO_4$) and screened under a Leica MZ25 fluorescence-equipped dissecting microscope with 100× magnification. Embryos with obvious morphological defects prior to 3 dpf were discarded. We scored the presence of retinal fibers in the tectum (particularly at 3 dpf), the trajectory of GFP-positive fibers in the optic tract, the width and shape of the optic tract, the density of tectal innervation, the size and shape of the tectal neuropil, the layer structure of the tectum, and the appearance of the RGC axonal meshwork in the tectal neuropil. Crosses in which a quarter of the F3 progeny showed a mutant phenotype were repeated. Two or three such re-tests were carried out before a mutant was considered a real candidate. In these cases, one or both of their parents were outcrossed to unrelated *Brn3c:mGFP* carriers to establish a mutant stock. The mutation was recovered in the next generation through random pairwise crosses. All mutants described in this report have been propagated as heterozygous stocks for at least three generations.

Immunohistochemistry

Mutant embryos/larvae were obtained by crosses of heterozygous carriers. Anaesthetized embryos/larvae were fixed in 4% paraformaldehyde (PFA) in phosphate-buffered saline. To enhance

permeability, PFA-fixed larvae older than 3 dpf were incubated in 0.1% collagenase in PBS. Incubation times for 3 dpf and 5 dpf were 45 minutes and 2 hours, respectively. For horizontal sections, embryos/larvae were cryoprotected in 30% sucrose/0.02% azide/PBS, embedded in OCT (Tissue-Tek, Sakura), and sectioned at 12 μm horizontally on a cryostat. The following antibodies and concentrations were used for whole-mount immunohistochemistry: anti-GFP, 1:40,000 (Molecular Probes); zn5, 1:1000 (Antibody Facility, University of Oregon); anti-acetylated tubulin, 1:2000 (Sigma); zpr-1, 1:200 (Developmental Studies Hybridoma Bank, University of Iowa); anti-phosphohistone H3, 1:500 (Upstate Biotechnology); and anti-parvalbumin, 1:1200 (Chemicon). TUNEL-based cell death assays were carried out according to manufacturer's instructions (In Situ Cell Death Detection Kit – Fluorescein, Roche).

Labeling of the retinotectal projection with carbocyanine dyes

Fish were deeply anesthetized in 0.016% tricaine (Sigma) and fixed in 4% PFA in PBS for 2-24 hours. They were embedded in 1% agarose in 0.5× PBS) and pressure injected with dye solution using a PV-820 pressure injector (World Precision Instruments, Sarasota, FL). The carbocyanine dye DiI (1,1′-dioctadecyl-3,3,3′,3′-tetramethylindocarbocyanine perchlorate, Molecular Probes D-282) was dissolved either in N,N-dimethylformamide (DMF) for fixed larvae or in ethanol for live larvae to a concentration of 2% (m/v). DiO (1,1′-dioctadecyl-3,3,3′,3′-tetramethyloxacarbocyanine perchlorate, Molecular Probes D-275) was dissolved in chloroform (2% m/v). To visualize the retinotectal map, DiI and/or DiO were injected into the eyes of larvae and imaged 12-24 hours later.

Confocal imaging

Larvae were embedded in a 0.5×20 mm imaging chamber (CoverWell, Grace Bio-labs) in 1.2% low melting point agarose dissolved in E3 medium containing 0.8% norepinephrine and 0.016% tricaine. For immunohistochemistry, the left eye was removed and stained embryos/larvae were mounted laterally in 70% glycerol in PBS. Confocal image stacks were acquired using either a BioRad 1024M or a Zeiss 510 META laser-scanning microscope. Long working distance objectives, 20× (air, NA 0.5) and 40× (water, NA 0.8), were used. To reconstruct axons and their arbors, a series of optical planes were collected (*z*-stack) and collapsed into a single image (maximum intensity projection) or rendered in three dimensions to provide views of the image stack at different angles. The step size for each *z*-stack was chosen upon calculation of the theoretical *z*-resolution of the objective used (typically 0.5-1 μm).

Results

Regulatory regions of *brn3c* drive stable expression of GFP in a subset of RGCs

We identified zebrafish *brn3c* (*brn3.1*, *pou4f3*) by PCR cloning. The putative amino acid sequence of Brn3c consists of 331 amino acids. Compared to mouse Brn3c, 81% of the amino acid positions are identical within the total sequence and 97% within the POU-domain. We confirmed the annotation by also cloning a highly related gene, *brn3b* (*brn3.2*, *pou4f2*) (DeCarvalho et al., 2004). A phylogenetic tree based on ClustalW sequence comparison (Higgins and Sharp, 1988) places the zebrafish Brn3b and Brn3c sequences into separate clades together with their mammalian orthologs (data not shown).

To generate a stable transgenic zebrafish line able to drive GFP expression in RGCs, we isolated about 6 kb of genomic sequence upstream of the *brn3c*-coding region and cloned it into a GFP expression vector (Fig. 1A) (see Materials and methods). Enhanced GFP, fused to the first 20 amino acids of GAP43, served as the marker gene, as described previously (Kay et al., 2004). The GAP43 sequence provides a membrane-targeting signal and ensures complete labeling of neurites (Zuber et al., 1989). Injection of the construct at the one-cell stage resulted in transient expression in select populations of neurons. Fish that showed bright expression in a large number of cells were raised to adulthood. Eighty-four injected fish were outcrossed against wild-type fish and analyzed for germline transmission. A total of 10 germline transgenic founder fish (12% of the injected embryos) were identified by visual inspection of their progeny under a fluorescence-

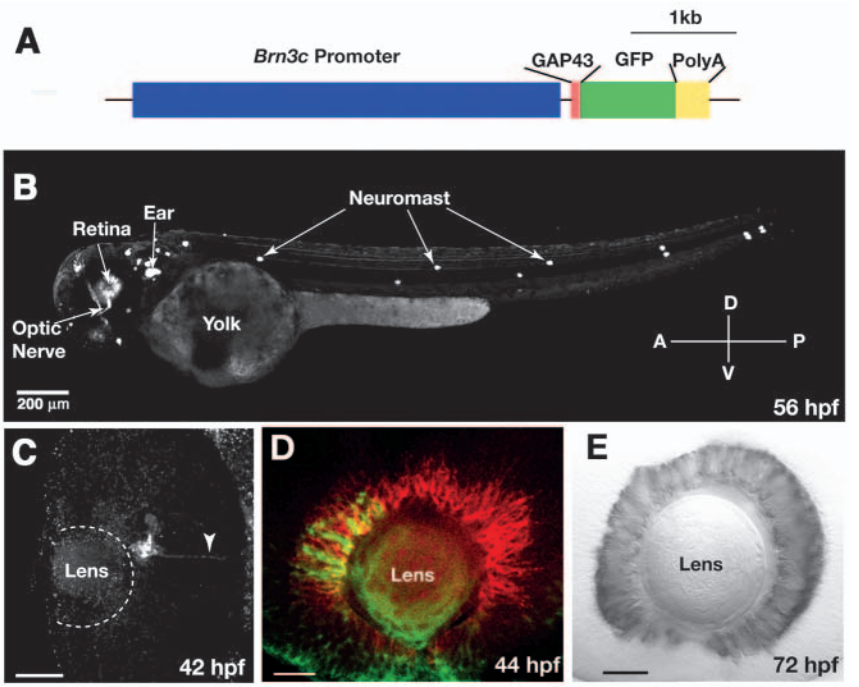

Fig. 1. A large subset of RGCs express GFP in the stable *Brn3c:mGFP* transgenic line. (A) Schematic drawing of the DNA construct used to generate the *Brn3c:mGFP* transgenic line. (B) Lateral view of 56 hpf live *Brn3c:mGFP* transgenic embryo showing GFP expression by RGCs and mechanosensory hair cells (neuromasts) of the lateral line and inner ear. The optic nerve is visible. (C-E) Fixed *Brn3c:mGFP* transgenic embryos labeled by whole-mount immunohistochemistry. (C) Ventral view of a 42 hpf retina, labeled with anti-GFP. Anterior (nasal) is upwards. GFP expression starts in a small cluster of cells in the ventronasal retina, near the optic fissure. The arrowhead indicates the first GFP-positive axons exiting the eye through the optic stalk. (D) Lateral view of a 44 hpf retina, labeled with anti-GFP in green and zn5 in red. GFP has spread into central retina. The onset of *Brn3c:mGFP* transgene expression follows that of zn5 by ~6 hours. (E) Lateral view of a 72 hpf retina, labeled with anti-GFP. GFP-positive RGCs are distributed uniformly throughout the ganglion cell layer. Scale bars: 200 μm in B; 20 μm in C-E.

equipped dissecting microscope. Offspring of these founder fish were raised to establish lines. The experiments described here were carried out in transgenic line *TG(Brn3c:mGFP)*^{s356t}.

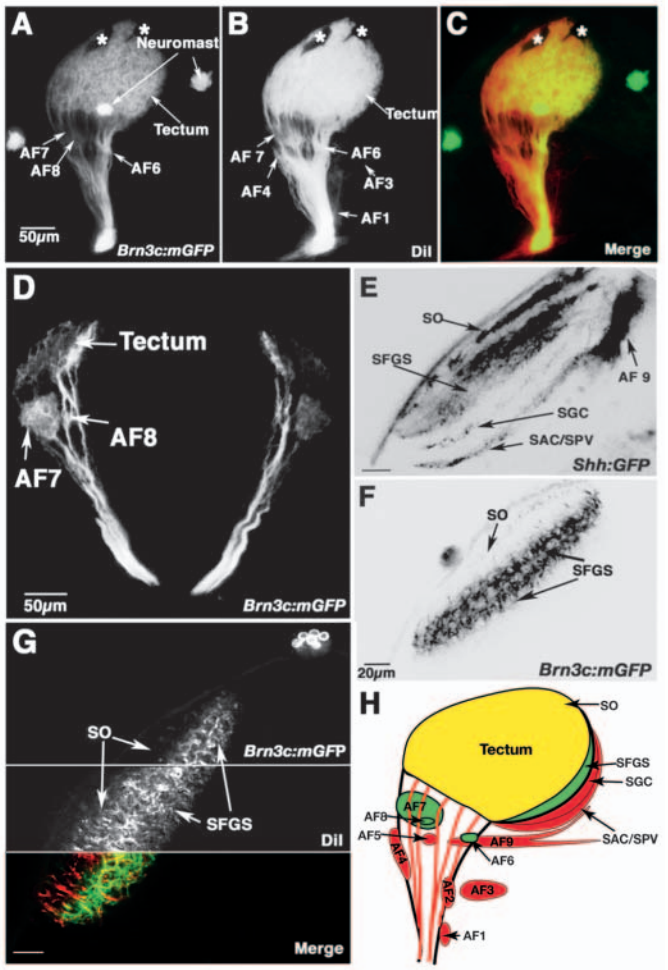

Fig. 2. The *Brn3c:mGFP* transgenic line reveals the architecture of the retinotectal projection. (A-C) Lateral view of the retinofugal projection in a 6 dpf fixed larva, whose eye has been removed (projection of a confocal *z*-stack). Specimen was only lightly fixed to preserve GFP label. (A) *Brn3c:mGFP* transgene expression. Four arborization fields, AF-6, AF-7, AF-8 and tectum (AF-10), are visible, as well as neuromasts of the lateral line. (B) Retinofugal projection, labeled with DiI following intraocular injection. (C) Merged view of the two labels shown in A and B. (D) Transverse section of 7 dpf *Brn3c:mGFP* transgenic larva, showing AF-7, AF-8 and the tectal layers. (E-G) Optical sections of tecta in 6 dpf live larvae (dorsal view; anterior is upwards, midline is towards the right). (E) *Shh:GFP* labels all four retinorecipient layers in the tectum. (F) *Brn3c:mGFP* labels the SO and SFGS. (G) Double-labeling in vivo with DiI and *Brn3c:mGFP*, showing the absence of GFP in one of the three SFGS sublaminae. For technical reasons, live DiI staining is always incomplete. As a result, some GFP-only (green) fibers are seen in the SFGS. (H) Summary of the *Brn3c:mGFP* labeling pattern. RGCs project to ten AFs. The largest AF, the tectum, has four layers. Only the green areas receive significant *Brn3c:mGFP* input. Red areas are devoid of GFP label. Yellow area (SO) is innervated mainly by non-GFP fibers, but also receives weak Brn3:mGFP innervation. AF, arborization field; SO, stratum opticum; SFGS, stratum fibrosum et griseum superficiale; SGC, stratum griseum centrale; SAC, stratum album centrale; SPV, stratum periventriculare; asterisks, melanophores in the skin. Scale bars: 50 μm in A-D; 20 μm in E-G.

All lines showed identical expression patterns, although positional effects on the levels of GFP expression were observed. At all stages, GFP is restricted to RGCs and to mechanosensory hair cells of the inner ear and lateral line neuromasts (Fig. 1B). The earliest GFP expression is observed at about 27 hpf in the inner ear. At about 42 hpf, GFP expression appears in a ventronasal patch of RGCs (Fig. 1C). In the hours that follow, the expression spreads over the entire extent of the retina, always restricted to a subset of RGCs and their processes and trailing the expression of DM-GRASP/neurolin, the epitope recognized by the zn5 antibody, by a few hours (Fig. 1C,D). The GFP-labeled cells are uniformly distributed within the ganglion cell layer (GCL) (Fig. 1E) and their axons approach the optic nerve head in multiple, distinct fascicles. At 5 dpf, ~50% of the RGCs are GFP positive, while 100% of them are labeled with zn5. The optic tract and the tectal neuropil are clearly demarcated (Fig. 2A,B). The label is stable to adulthood (not shown).

Brn3c:mGFP labels a distinct subset of RGCs with defined target specificity

We next asked if the *Brn3c:mGFP* transgene could be used to visualize the architecture of the retinotectal projection in zebrafish larvae. RGCs project axons to ten target areas in zebrafish, of which the tectum is the largest. These areas have been referred to as retinal arborization fields (AFs) and are numbered according to their proximodistal position along the optic tract (Burrill and Easter, 1994). The tectum was named AF-10, being the most distal retinorecipient area. *Brn3c:mGFP*-expressing axons were found to strongly innervate the tectum and, more sparsely, AF-6, AF-7 and AF-8 (Fig. 2A,D). GFP-labeled fibers are almost completely absent from AF-4, AF-5 and AF-9, and were not detected in AF-1, AF-2 and AF-3 (Fig. 2A-C; data not shown).

In the tectum of adult cyprinids, four major retinorecipient layers have been described: the *stratum opticum* (SO), the *stratum fibrosum et griseum superficiale* (SFGS), the *stratum griseum centrale* (SGC) and the boundary zone between *stratum album centrale* and *stratum periventriculare* (SAC/SPV) (Meek, 1983; Vanegas and Ito, 1983; von Bartheld and Meyer, 1987). Whole-eye DiI fills reveal that these four retinorecipient layers are already present in 6 dpf larvae. The same four layers are seen in a *Shh:GFP* transgenic line (Neumann and Nuesslein-Volhard, 2000), in which many RGC axons are unselectively labeled (Roeser and Baier, 2003) (Fig. 2E). The most superficial layer, the SO, is about 10 μm thick, densely labeled and begins at the rostral pole of the tectum. The layer below, the SFGS, is 30 μm thick and is divided into three sublaminae. The two deeper layers, SGC and SAC/SPV, are more sparsely innervated. At 6 dpf, these two layers extend further caudally than the two superficial layers. In zebrafish larvae, unlike birds and mammals, axons enter their target layer right at the entrance of the tectum; only a subset of the fibers projects to the SO and these are not seen 'diving down' into the tectum terminating in the deeper layers (data not shown).

In contrast to *Shh:GFP* and DiI fills, the vast majority of *Brn3c:mGFP*-labeled axons project to the SFGS, and here only to the two deeper sublaminae (Fig. 2F). The projection to SO is very sparse. The paucity of *Brn3:mGFP* axons in SO suggests that only a small subset of the axons in SO originate from *Brn3c:mGFP*-expressing RGCs (Fig. 2G). SGC and

Table 1. Summary of retinotectal mutants identified in the *Brn3c:mGFP* screen

Gene (abbreviation)	Alleles	Retina	Background adaptation*	Other phenotypes	Viability (maximal age)
Reduced number of retinal axons					
daredevil (*ddl*)	*s563*	Fewer RGCs, wider ciliary margin, fewer PhR	Dark	Heart conductivity defect, swimbladder not inflated	6 dpf
Delayed innervation of the tectum					
vertigo (*vrt*)	*s1614*	Normal	Dark	Balance deficit, swimbladder not inflated	10 dpf
late bloomer (*late*)	*s551*	Normal	Normal	None detected	Adult
tarde demais (*tard*)	*s587*	Normal	Mildly dark	Swimbladder not inflated	14 dpf
Laminar specificity defect					
dragnet (*drg*)	*s510*, *s530*	Normal	Mildly dark, variable	Lens covered by extra cells	Adult
Deficient confinement of axons to tectal neuropil					
fuzz wuzzy (*fuzz*)	*s531*	Normal	Mildly dark	Swimbladder not inflated	10 dpf
beyond borders (*beyo*)	*s578*	'Smiling' IPL at margin	Mildly dark	Reduced forebrain, swimbladder not inflated	10 dpf
breaking up (*brek*)	*s574*	RGC axon degeneration	Dark after 5 dpf	Swimbladder not inflated	10 dpf
Disorganized fascicles in the tectum					
blue kite (*bluk*)	*s582*	Normal	Dark	Swimbladder not inflated	10 dpf
clewless (*clew*)	*s567*	Normal	Mildly dark	Lens degeneration	Adult
blind date (*blin*)	*s573*	Normal	Mildly dark, recover after 7 dpf	None detected	Adult
coming apart (*coma*)	*s532*	Misplaced RGCs at ciliary margin	Normal	Swimbladder not inflated	10 dpf

*Background adaptation is a crude indicator of visual function (Neuhauss et al., 1999). Visually impaired fish are often unable to measure ambient light levels and are dark, owing to dispersal of melanin pigment in their skin.
IPL, inner plexiform layer.

SAC/SPV do not receive *Brn3c:mGFP*-labeled input. In summary, these labeling studies show that the *Brn3c:mGFP* transgene labels a distinct subpopulation of RGCs with restricted target specificity (Fig. 2H). Therefore, *Brn3c:mGFP* reveals details of the retinotectal architecture that would be masked by an unselective RGC stain. We employed this line next in a small-scale screen in search of new retinotectal mutants.

Overview of the screen

For the screen, we mutagenized the spermatogonia of 17 adult male zebrafish with ENU and outcrossed them to non-mutagenized females. The mutation rate was determined to be about 0.3% per gene per haploid genome. We used the pigmentation gene *sandy* (tyrosinase) as the specific locus for its easily detectable phenotype (Page-McCaw et al., 2004). The F1 fish were then crossed to *Brn3c:mGFP* carriers to generate 233 F2 families. A total of 1303 crosses were screened by visual inspection of the GFP-labeled retinotectal projection. Based on the varying number of crosses per individual F2 family (average 5.6, corresponding to 0.8 genomes), we calculated that our screen encompassed 168 genomes (Mullins et al., 1994).

The screen was carried out on F3 progeny at 3 dpf and again at 6 dpf. These two developmental stages are particularly informative for revealing perturbations in the retinotectal projection. In wild type, RGC axons reach the anteroventral boundary of the tectum at 48 hpf. One day later, at 72 hpf (3 dpf), RGC axon arbors reach the posterodorsal boundary of the tectum and completely cover the tectum (Stuermer, 1988). Thus, screening at 3 dpf enabled us to uncover mutations disrupting the initial stages of the retinotectal projection. Between 3 dpf and 6 dpf, RGC axonal arbors elaborate synaptic connections with tectal neurons. Screening at 6 dpf thus allowed us to discover mutations affecting the refinement and maintenance of the retinotectal projection.

Progeny of crosses from 65 F2 families initially showed a putative mutant phenotype and were re-screened by mating the same pair and scoring their F3 progeny again. Less than one third of these (21) were confirmed and outcrossed to *Brn3c:mGFP* transgenic wild type. All but two mutants were recovered in the next generation. However, six were considered unspecific upon closer inspection and discarded. The discarded mutants had smaller tecta or smaller eyes, owing to degeneration or early developmental problems. All mutants were sectioned at 6 dpf and examined histologically using DAPI to highlight cytoarchitecture of retina and tectum, in conjunction with anti-GFP. Two mutations with similar phenotypes were found to be alleles of the same gene by complementation analysis. As described below, we discovered 13 mutations in 12 genes, which have been grouped into five classes (Table 1). All mutants are recessive, completely penetrant with respect to their axon phenotype and are transmitted in Mendelian ratios. Their phenotypes uncover largely unexplored processes in the assembly of neural architecture.

The *daredevil* (*ddl*) gene is important for the differentiation of most RGCs

We identified a mutant, *ddl*, showing a severe reduction of retinal axons that innervate the tectum at 3 dpf (Fig. 3A,B). The optic tract is thin, and RGC axons do not cover the entire tectum. Closer investigation revealed that the primary defect of this mutant is in generating RGCs. Between 42 and 48 hpf, when newly differentiating RGCs begin to express *Brn3c:mGFP* in wild type, GFP expression in the *ddl* retina is sparse. This is in contrast to GFP expression in hair cells, which is comparable with wild type in strength and time of

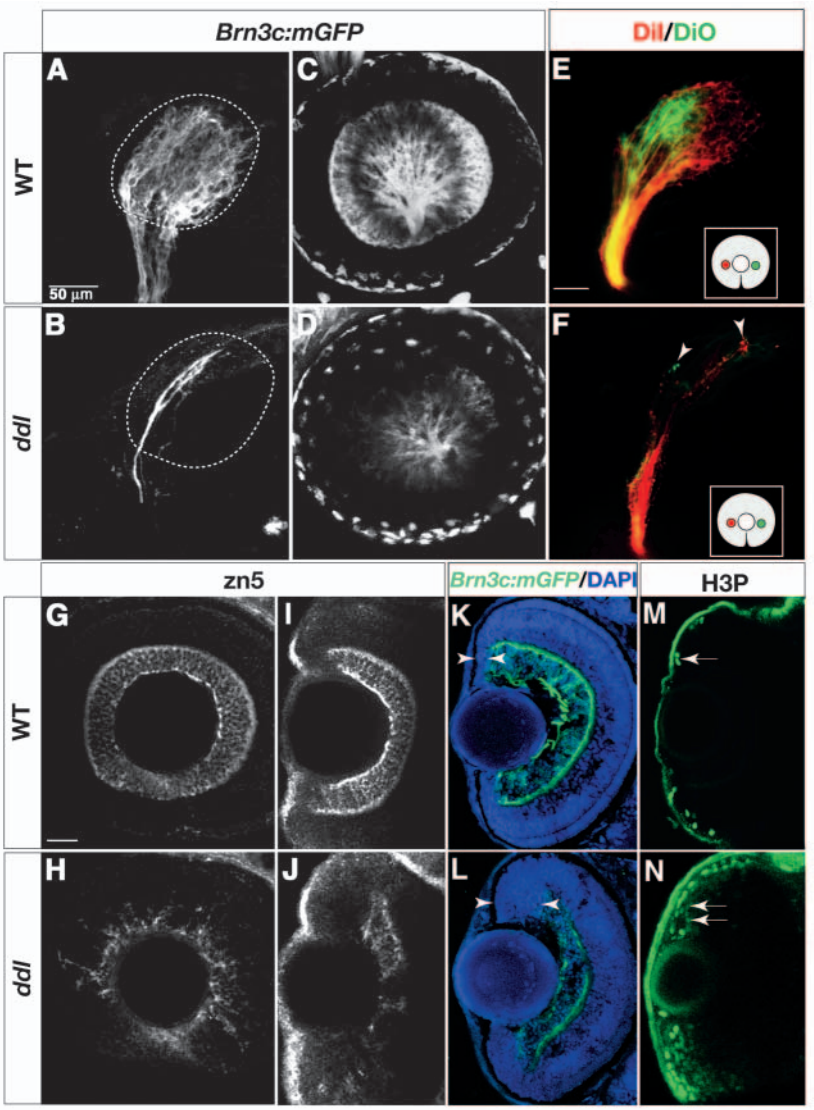

Fig. 3. *daredevil* (*ddl*) mutants have fewer RGCs. Analysis of cell-type markers in wild type (A,C,E,G,I,K,M) and *ddl* (B,D,F,H,J,L,N). (A,B) Lateral views of 78 hpf tecta, labeled with whole-mount anti-GFP. Broken lines outline boundaries of the tectal neuropil. The wild-type tectum (A) is covered by axons. Few axons can be detected in the *ddl* tectum (B). (C,D) Confocal images of retinas in live 60 hpf embryos. The number of GFP-positive RGCs is greatly reduced in *ddl* (D). (E,F) Analysis of the retinotopic map in 72 hpf wild type (E) and *ddl* (F). DiI (red) and DiO (green) were pressure injected into nasal and temporal retina, respectively (see inserts for illustration of retinal injection sites). The gross topography of axon targeting in *ddl* mutants is not affected, with nasal axons still projecting to the posterior tectum and temporal axons to the anterior tectum (F). (G-J) Whole-mount Zn5 staining of 72 hpf retinas. (G,H) Lateral views. (I,J) Dorsal views. The number of zn5-positive RGCs is greatly reduced in *ddl*. (K,L) Sections of 78 hpf retinae, labeled with anti-GFP (green) and DAPI (blue). The ciliary margin (between arrowheads) in the *ddl* retina is wider than in wild type. (M,N) Dorsal views of 72 hpf whole-mount retinae, labeled with anti-phosphohistone H3 (H3P). The number of dividing cells (arrows) is greatly increased at the ciliary margin in *ddl*. Scale bars: 50 μm in A and E (for tectum panels); 20 μm in G (for retina panels).

onset (data not shown). After 60 hpf, when wild-type retina is uniformly filled with GFP-positive RGCs, the *ddl* retina contains less than 10% of the GFP-positive population (ranging from three to a few dozen individual RGCs scattered over the retina) (Fig. 3C,D). The few remaining RGCs send out axons, projecting in a straight course to the tectum and reach the target before and around 3 dpf, the same time as wild type (Fig. 3A,B). We asked if the retinotopic map was intact, despite this dramatic depletion of RGCs. Following injection of DiI into the nasal retina and DiO into the temporal retina of an aldehyde-fixed wild-type larva (3 dpf), we observed that nasal axons invariably projected to the posterior tectum and temporal axons to the anterior tectum (Fig. 3E), as reported before (Stuermer, 1988; Baier et al., 1996). Perhaps surprisingly, given the sparse filling of the tectum, this topographic relationship is retained in *ddl* mutants (Fig. 3F).

To test whether only the Brn3c-expressing subpopulation was reduced, we stained the 3 dpf retina with zn5 and HuC antibodies, which label all RGCs (zn5) or RGCs and amacrine cells (HuC). This experiment showed that most RGCs are absent in *ddl* mutants (Fig. 3G-J). Amacrine cells are also reduced in number (data not shown). DAPI staining further suggested that photoreceptors are undifferentiated, but overall retinal lamination is unaffected (Fig. 3K,L). The ciliary margin of this mutant is enlarged (Fig. 3I-L) and anti-phospho-histone H3 labeling demonstrated an increase in the number of mitotically active progenitors in this region (Fig. 3M,N). At 3 dpf, *ddl* mutants have normal body morphology and are indistinguishable from their wild-type siblings, except for their retina phenotype. After 3 dpf, the eye is visibly smaller, and the swimbladder fails to inflate. At about 3.5 dpf, the hearts of *ddl* mutants begin to show arrhythmia, suggestive of a conductivity defect. At 4 dpf, mutants can be sorted based on pericardial edema; they die at around 6 dpf.

Innervation of the tectum is delayed in *vertigo* (*vrt*), *tarde demais* (*tard*), and *late bloomer* (*late*) mutants

At 72 hpf, RGC axons already occupy the entire tectal neuropil. However, the tectum is immature at this stage and retinorecipient layers are not detectable. Large growth cones are seen, and axon arbors appear to spread out without the characteristic adhesion between branches, which is seen later on (see below). Three mutants, vrt^{s1614}, $tard^{s587}$ and $late^{s551}$, were found to have few if any arbors in the tectum at 3 dpf, although tectal architecture (as judged by DAPI histology) appears normal. Strikingly, the retinotectal projection in these mutants recovers later on.

vrt mutants exhibit the most severe delay. Once reaching the boundary of the tectum, RGC axons stall (Fig. 4A,B). After 4 dpf, the axons resume their growth into the tectum, which they eventually cover completely (Fig. 4C-F). Prior to 3 dpf, RGC differentiation and axon pathfinding are normal and on schedule (Fig. 4G,H). The number of RGCs, expressing GFP

or stained with the zn5 antibody, is identical to wild type, and their axons follow the normal path across the midline and towards the tectum. This suggests that the *vrt* mutation specifically impairs one particular stage of axon growth: the entry into the tectum. Interestingly, the optic tract is noticeably wider in *vrt* mutants. The thickening of the optic tract could be the result of reduced fasciculation or of excessive backbranching by axons that are stalled at the anterior pole of the tectum. *vrt* mutants lack a swimbladder and die at around 10 dpf.

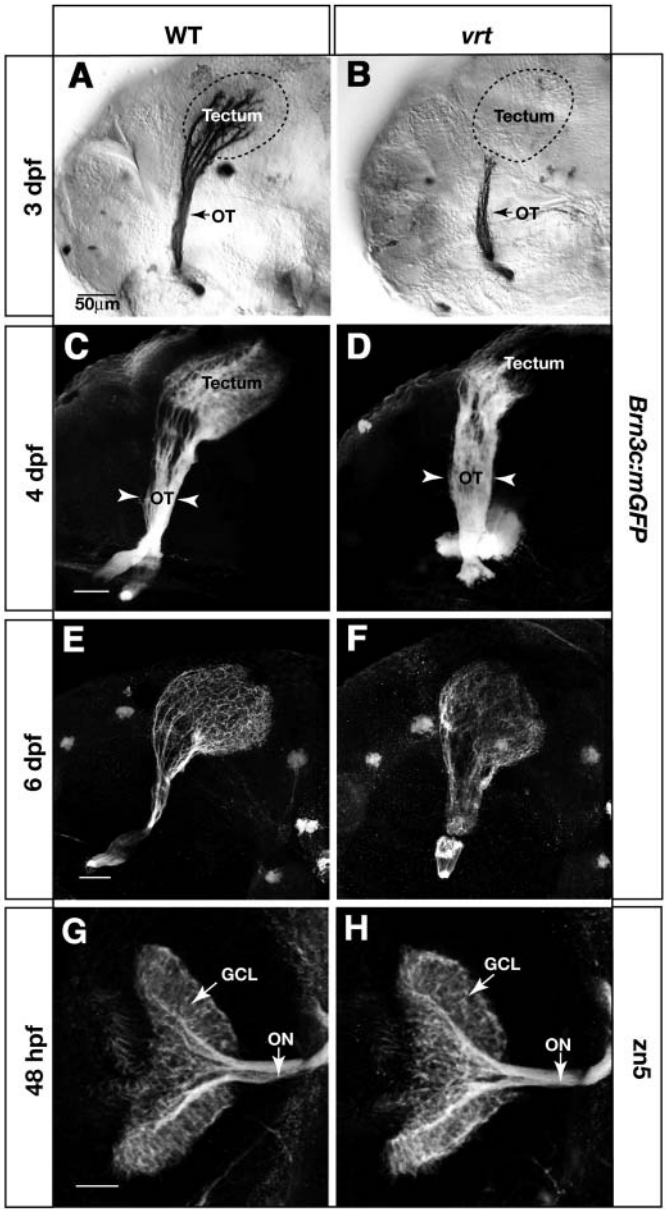

Fig. 4. *vertigo* (*vrt*) mutants show severely delayed innervation of the tectum. Analysis of retinal axon projection in wild type (A,C,E,G) and *vrt* mutants (B,D,F,H). (A-F) Lateral views of the retinotectal projection in *Brn3c:mGFP* transgenic fish, labeled with anti-GFP. At 3 dpf, the wild-type tectum (A) is fully innervated, while the *vrt* tectum (B) is devoid of axons. Broken lines outline the tectum boundaries. In 4 dpf wild-type larvae (C), the density of axon arbors is increased compared with 3 dpf (A), and dorsal and ventral branches are clearly visible in the optic tract. In *vrt* (D), axons have invaded the anterior tectum, and the optic tract (OT) is abnormally wide (arrowheads). At 6 dpf, axons innervate the whole tectum in the *vrt* mutant (F) similar to wild type (E) The optic tract remains wider than normal. (G,H) Dorsal views of 48 hpf retinas and optic nerves, labeled with zn5. The number of RGCs and their axons is similar between wild type (G) and *vrt* (H). Scale bars: 50 μm.

tard and *late* mutants display a milder delay of the retinotectal projection than *vrt*. At 3 dpf, axon arbors can be observed in anterior tectum, but not in posterior tectum (Fig. 5A-C). The optic tracts are morphologically normal at all times. RGC axon growth recovers by 4 dpf, and at 6 dpf the tectum is completely covered by fibers (Fig. 5D-F). The tectal neuropil in *tard* mutants retains an abnormal shape and its margins are less delineated than in wild type (Fig. 5E). *tard* mutants fail to inflate their swim bladders and die at around 2 weeks of age. By contrast, *late* mutants are morphologically inconspicuous, including their tectum (Fig. 5F), have swim bladders and are adult viable. In fact, they can only be distinguished from their wild-type siblings by the delayed innervation of the tectum around 3 dpf.

Lamination of retinal input is disrupted in *dragnet* (*drg*) mutants

We identified two alleles, drg^{s510} and drg^{s530}, of a gene important for targeting retinal axons to the appropriate tectal layer. drg^{s530} results in a somewhat weaker phenotype than drg^{s510}. In wild-type zebrafish larvae, most axons extend directly into a specific layer at the entrance of the tectum and remain confined to the chosen layer (data not shown). *Brn3c:mGFP*-labeled RGCs project mostly to the two deep sublaminae of the SFGS, and the SO is only lightly labeled (see Fig. 2F,G; Fig. 6A,C). In *drg* mutants, this pattern of laminar targeting is perturbed (Fig. 6B,D). Ectopic fascicles, 2-4 μm in diameter, are observed in the SO, apparently displaced from the SFGS. GFP-labeled axons travel between the two layers. The entire tectum is innervated in this mutant, and both tectal cytoarchitecture (by DAPI histology; data not shown) and retinotopic mapping are intact (Fig. 6E,F). The lamination defects are detectable as early as 3.5 dpf and are specific to the tectum. Sublaminar targeting of amacrine processes and of RGC dendrites in the inner plexiform layer of the retina is normal, as shown by anti-parvalbumin and anti-GFP double-labeling (Fig. 6G-N). The only other detectable phenotype of *drg* mutants is an opaque lens after 5 dpf, caused by overgrowth by epithelial cells (Fig. 6G,H). *drg* mutants are fully viable as adults.

Neuropil boundaries dissolve in *fuzzy wuzzy* (*fuzz*), *beyond borders* (*beyo*) and *breaking up* (*brek*) mutants

In $fuzz^{s531}$, $beyo^{s578}$ and $brek^{s574}$ mutants, the retinotectal projection forms on time and is initially indistinguishable from wild type, but the density of axon arbors is reduced after 5 dpf. Optic tracts are of normal width and show the characteristic branching pattern, as the RGC fibers enter the tectum. This suggests that the normal complement of axons is present, but that their arbors are smaller or have fewer branches. The borders of the retinotectal fiber zone are less well demarcated ('fuzzy') in these mutants, with axons and growth cones frequently straying outside the neuropil area (Fig. 7). Tectal cytoarchitecture is unaltered, as determined by DAPI staining.

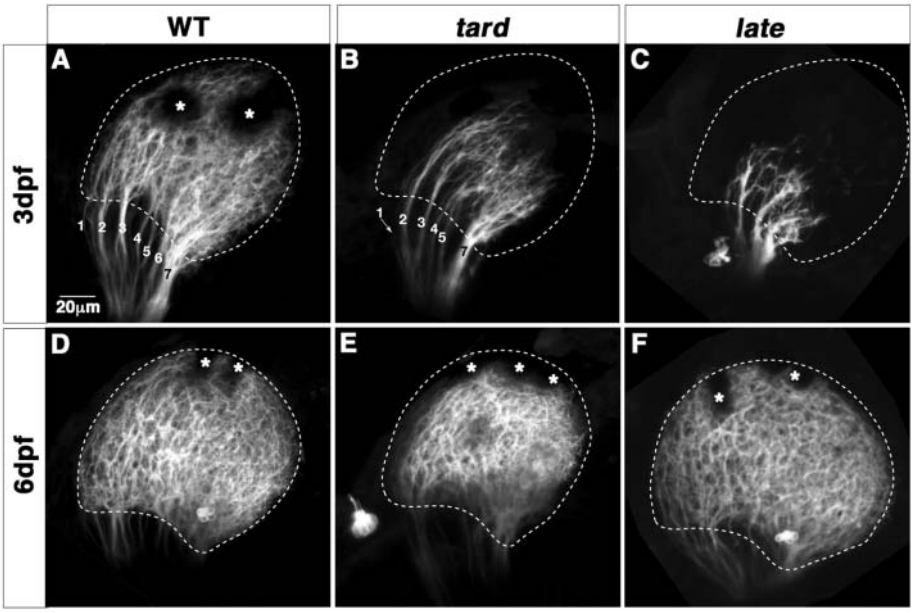

Fig. 5. *tarde demais* (*tard*) and *late bloomer* (*late*) mutants show mildly delayed innervation of the tectum. (A-F) Confocal images of *Brn3c:mGFP* labeled retinotectal projections of 80 hpf tecta in live larvae (A-C). The wild-type tectum (A) is filled with retinal axons. The optic tract has branched into stereotyped fascicles, labeled with numbers. The *tard* tectum (B) and the *late* tectum (C) are less than halfway innervated. (D-F) Lateral views of 6 dpf tecta. The *tard* tectum and the *late* tectum are now covered with axons. However, the *tard* tectum is small and its boundary remains abnormal (E), compared with wild type (D) and in contrast to *late* (F). Asterisks indicate melanophores on the skin. Broken lines outline the tectal neuropil. Scale bars: 20 μm.

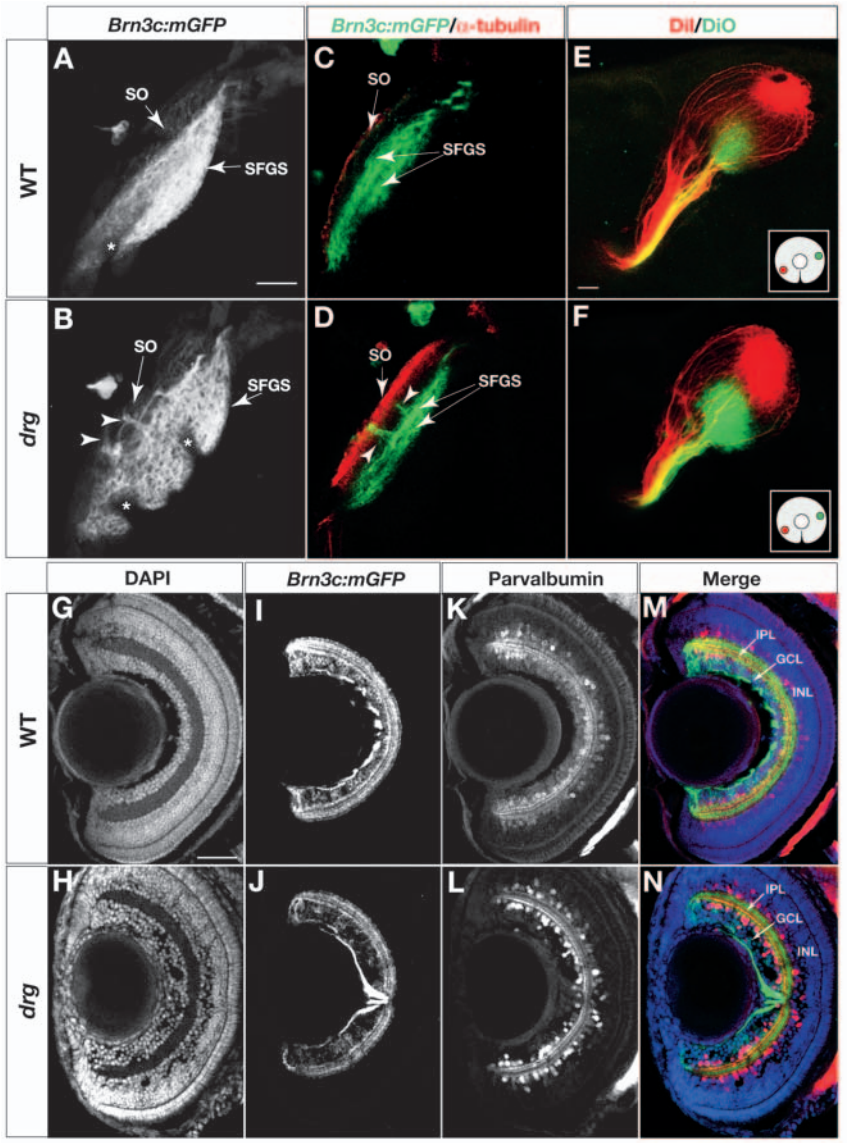

Fig. 6. Laminar specificity is perturbed in *dragnet* (*drg*) mutants. (A-D) Analysis of retinorecipient layers in 6 dpf wild type (A,C) and *drg* (B,D). (A,B) *Z* projections of confocal image stacks, labeled with *Brn3c:mGFP*. Larvae are mounted at a slightly oblique angle to better visualize the gap between SO and SFGS. (C,D) Optical sections of *Brn3c:mGFP* tecta, stained with whole-mount anti-acetylated tubulin (red) and anti-GFP (green). Arrowheads indicate ectoptic axon fascicles traveling between SO and SFGS in *drg* mutants. (E,F) Analysis of the retinotopic map in 6 dpf wild type (E) and *drg* (F). DiI (red) and DiO (green) were pressure injected into ventronasal and dorsotemporal retina, respectively (see inserts for illustration of injection sites). Axon targeting in *drg* (F) is comparable with wild type (E), suggesting that positional information along the retinotopic axes is intact. (G-N) Analysis of the inner plexiform layer (IPL) in sections of 6 dpf retina (see M,N for labels of retinal layers). (G,H) DAPI labeling. (I,J) Anti-GFP labeling to visualize the four sublaminae to which *Brn3c:mGFP* RGC dendrites project. (K,L) Anti-parvalbumin labeling, to highlight a subpopulation of amacrine cells that project to three sublaminae in the IPL. (M,N) Triple-labeling (merged image) showing DAPI (blue), anti-GFP (green) and anti-parvalbumin (red). Formation of IPL sublaminae is not affected in *drg*. An apparently unrelated phenotype of *drg* can be seen using the DAPI stain: an abnormal aggregation of cells in front of the *drg* lens (H). Asterisks indicate melanophores in the skin. Scale bars: 20 μm in A,G.

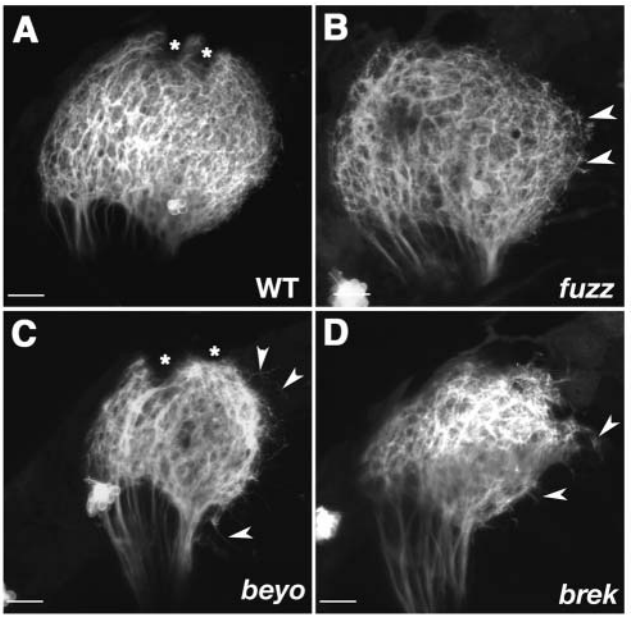

Fig. 7. Tectal neuropil boundaries dissolve in *fuzz wuzzy* (*fuzz*), *beyond borders* (*beyo*) and *breaking up* (*brek*) mutants. (A-D) *Z*-projections of confocal image stacks showing lateral views of tecta in 6 dpf live *Brn3c:mGFP* larvae. The boundary of the tectum is smooth and well defined in wild type (A). In *fuzz* (B), axon arbors are less dense in the tectal neuropil and often overshoot the tectal boundary (arrowheads). The overshooting phenotype is more severe in *beyo* (C) and *brek* (D). Asterisks indicate melanophores. Scale bars: 20 μm.

In *brek* mutants, the GFP label in the tectal neuropil becomes punctate after 4 dpf, sometimes as late as 6 dpf, indicating that axons are disintegrating in this mutant (see Fig. S1 in the supplementary material). In a substantial proportion of fish, axon degeneration is uneven, with one region of the tectum initially more affected than another, although a time-course analysis showed that the temporal pattern is inconsistent between animals (n=6). We could not detect an excessive number of TUNEL-positive cells in the mutant retina at 5 dpf, suggesting that axon retraction is not secondary to RGC death in the retina (data not shown). The axon degeneration phenotype is not seen in *fuzz* or *beyo*. In *beyo* mutants, the inner plexiform layer of the retina is misshaped at the margins, bending distally to the outer nuclear layer (see Fig. S2 in the supplementary material), and the telencephalon is reduced (data not shown). All three mutants do not inflate their swimbladders and die as young larvae.

Fiber organization is disrupted in *clewless* (*clew*), *blue kite* (*bluk*), *coming apart* (*coma*) and *blind date* (*blin*) mutants

In wild type, axons are sorted in the optic tract according to their topographic position and enter the tectum through a set of stereotyped fascicles (Stuermer, 1988) (see Fig. 5C). After entering the tectum, axon arbors do not spread uniformly, but rather form a characteristic grid within the neuropil, with regions of high fiber density evidently separated by gaps. Thick fascicles circle the perimeter of the tectum, from which single axons depart at various positions to navigate to their respective targets in the center of the neuropil. Thin fascicles are also observed traveling through the wild-type tectum. This organization becomes evident in confocal images of *Brn3c:mGFP* tecta at high magnification (Fig. 8A,B).

In a heterogeneous group of four mutants, *clew*^{s567}, *coma*^{s532}, *bluk*^{s582} and *blin*^{s573}, the RGC fibers are more diffuse and less mesh-like than in wild type (Fig. 8C,D), or appear to meander in the neuropil (Fig. 8E,F). We interpret the ‘diffuse’ phenotype as a lack of fiber-fiber adhesion, but the apparent dispersion may have other causes as well. Although tectal cytoarchitecture appears overall normal (by DAPI histology), the tectum is slightly smaller in *coma* and *bluk*. In *coma* mutants, the optic tract is already disorganized upon entering the tectum: axons preferentially join the dorsal and ventral branches and appear to avoid the more centrally positioned fascicles (Fig. 8F). The fascicles circling the tectum are also thicker and more compact. However, DiI and DiO double-labeling of RGC axons originating from the nasoventral and temporodorsal quadrants, respectively, demonstrated that the retinotopic map is intact (data not shown). The *coma* mutant also has a specific retinal defect: a small number of the newborn RGCs at the ciliary margin are mispositioned in the distal retina near the inner nuclear layer. These cells express GFP at the same intensity as regularly positioned RGCs and exhibit a neuronal morphology (see Fig. S2 in the supplementary material). The *coma* and *bluk* mutations are larval lethal, while *blin* and *clew* mutants are adult viable.

Discussion

We generated a transgenic zebrafish line that expresses membrane-targeted GFP under control of a *brn3c* enhancer fragment. Brn3c is a POU-domain transcription factor, which is involved in RGC differentiation and axon outgrowth (Liu et al., 2000; Wang et al., 2002). The *Brn3c:mGFP* transgene is expressed in a subset of RGCs and in mechanosensory hair cells, similar to endogenous *brn3c* (DeCarvalho et al., 2004; Erkman et al., 1996; Xiang et al., 1995). The optical transparency of zebrafish embryos and larvae allowed us to visualize the retinotectal projection in living fish, relying solely on the crisp labeling of RGC axons by membrane-bound GFP. We could thus investigate, at unprecedented resolution, tectal neuropil organization, layer formation, fasciculation and the time course of innervation in both wild-type and mutant zebrafish. A screen of 168 ENU-mutagenized genomes in the *Brn3c:mGFP* background revealed 13 mutations disrupting the orderly innervation of the tectum (Fig. 9). The affected genes may be expressed in the RGCs or the tectum, or both. The newly discovered mutant phenotypes can be categorized into five groups (Table 1), none of which has, to our knowledge, been described before.

We designed our new GFP-based screen to find phenotypes that would have escaped discovery in the earlier screen (Karlstrom et al., 1996; Trowe et al., 1996) or would have been difficult to analyze in sufficient detail using carbocyanine tracing alone (Burrill and Easter, 1994; Kaethner and Stuermer, 1992; Stuermer, 1988). We concentrated on mutations disrupting the fine architecture and temporal coordination of the retinotectal projection, taking advantage of the highly reproducible label afforded by a genetically encoded reporter, by its stability, and by its cell-type specific expression pattern.

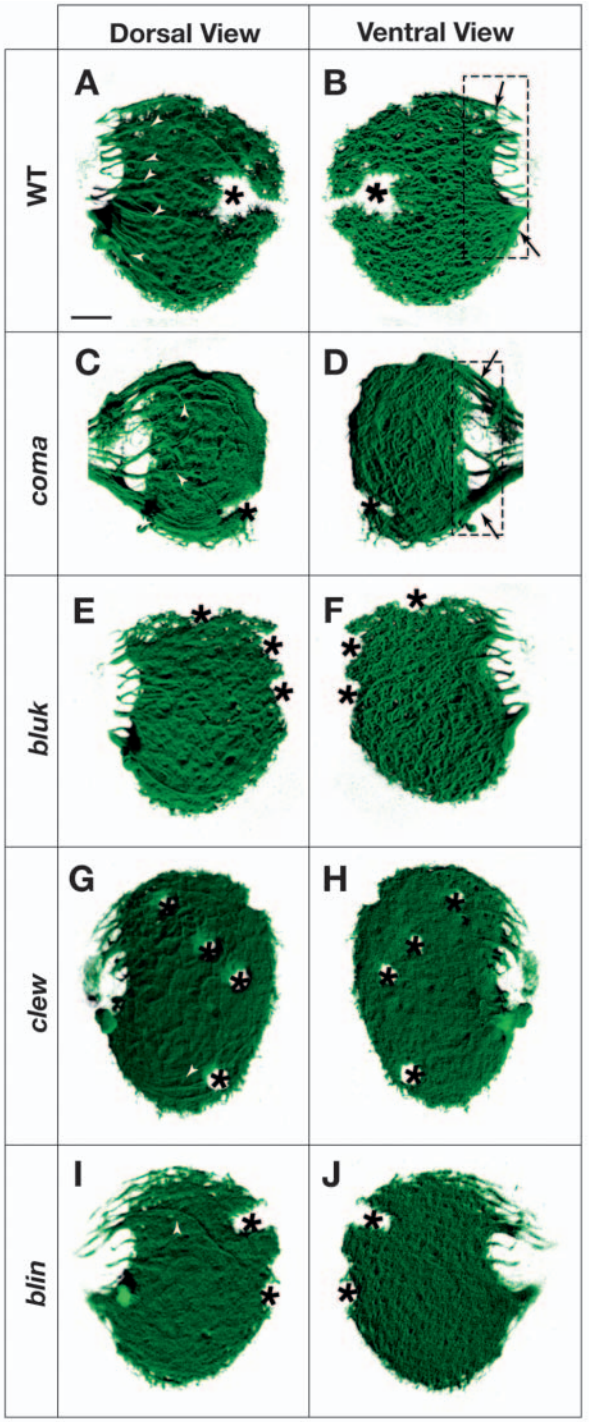

Fig. 8. Fasciculation is disorganized in *blue kite* (*bluk*) and *coming apart* (*coma*), *blue kite* (*bluk*), *clewless* (*clew*) and *blind date* (*blin*) mutants. (A-F) Surface-rendered 3D reconstructions of confocal images taken from 6 dpf live *Brn3c:mGFP* larvae. Dorsal views (A,C,E,G,I) and mirror-image ventral views (B,D,F,H,J) of the same tecta are shown. On the dorsal surface, axon fascicles are visible within the tectal neuropil of wild type (A) (arrowheads). The ventral view (B) demonstrates the characteristic dense grid of arbors. (C,D) In *coma*, fascicles both in the optic tract (hatched rectangle in D) and in the neuropil are disorganized. (E-J) In *bluk*, *clew* and *blin*, fascicles within the neuropil are greatly reduced (E-I) and axon termations appear diffuse. Asterisks indicate melanophores in the skin. Scale bars: 20 μm.

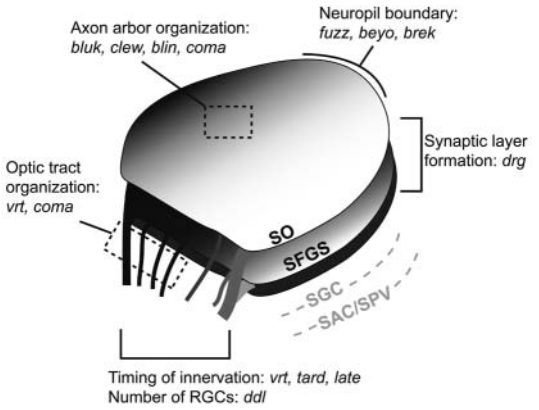

Fig. 9. Summary of retinotectal mutants. The 13 loci are predicted to affect different aspects of tectal development and architecture. The *ddl* protein is required for differentiation of most RGCs. The *vrt*, *tard* and *late* gene products ensure timely innervation of the tectum. Products of *vrt* and *coma* organize the fascicles in the optic tract, while *bluk*, *clew*, *blin* and *coma* regulate fiber-fiber interaction in the tectum. Proteins encoded by *fuzz*, *beyo* and *brek* confine axons to the neuropil, while *drg* is required for targeting axons to the SFGS. (The deeper layers of the tectum, SGC and SAC/SPV, are not labeled by *Brn3c:mGFP*.)

Although the scale of our new screen was less than one-tenth of the original retinotectal screen, it was very productive in detecting specific phenotypes. The previous screen had enriched for mutants with pleiotropic phenotypes. As a result, of the 114 mutants described, all but eight (7%) die as young larvae, indicating pervasive, non-visual defects. For comparison, of the 13 new mutants, five are adult viable (39%) and most of them show few if any phenotypes outside the visual system (Table 1).

Our screen was preordained to find mutations disrupting RGC differentiation, as these are sure to prevent, or perturb, axonal projections to the tectum. In fact, one mutant (*ddl*) with sparse innervation of the tectum, was shown to produce only a fraction (less than 10%) of the normal complement of RGCs. The transcription factor Brn3b is required for differentiation, pathfinding and survival of RGCs, and might therefore be a candidate gene for *ddl* (Erkman et al., 2000; Liu et al., 2000). However, the few remaining RGCs, which are spared in *ddl* mutants, are able to extend axons into the tectum in a straight course, suggesting that pathfinding is normal. Moreover, other organs, such as the heart, are also affected, arguing against *brn3b* as a candidate gene. *ddl* is also distinct from *lakritz/ath5*, whose mutation leads to a complete loss of RGCs, but otherwise milder retinal defects (Kay et al., 2001; Kay et al., 2004). The unique combination of phenotypes, together with its genetic map position (T.X., unpublished), suggests that *ddl* encodes a gene not previously implicated in RGC development.

In wild type, the first RGC axons enter the tectum at 48 hpf and reach its posterior end within the next 24 hours (Stuermer, 1988). The larvae display their first visual reflexes at around the same time, suggesting that synaptogenesis is rapid (Easter and Nicola, 1996). We discovered three genes, *vrt*, *tard* and *late*, important for keeping innervation of the tectum on this tight schedule. In these mutants, axons stall at the anterior end of the tectum and invade it after a substantial delay. The

mutations may disrupt extracellular signals that regulate innervation of the tectum, or a component of the transduction machinery that transmits these signals inside the growth cone and links them to the cytoskeleton. Blocking FGF signaling in the *Xenopus* retinotectal projection results in a bypass phenotype, where RGC axons grow around the tectum (McFarlane et al., 1996; Walz et al., 1997). This is different from the stalled growth we observed here in zebrafish *vrt* mutants. Alternatively, one or more of these genes may encode a factor required for axon elongation, such as a cytoskeletal or motor protein. Strikingly, the defects are only transient – by 6 dpf, the retinotectal projection has recovered – and appear to be specific to the optic tract/tectum boundary along the visual pathway. Although a retinotectal map forms eventually, these mutants remain completely (*vrt*) or partially blind (*tard*, *late*) (T.X., unpublished). It will be interesting to find out if these persistent visual impairments are secondary to the delayed innervation or caused by a direct effect on visual functions by the respective gene products.

Axon-axon interactions are important for assembling a highly organized neural structure and for maintaining its integrity. As the optic tract merges with the anterior border of the tectal neuropil, retinal axons are ordered into a stereotyped set of fascicles (von Bartheld and Meyer, 1987). About ten thin fascicles emanate from two thicker branches, the dorsal (medial) and the ventral (lateral) brachia of the optic tract, which mainly contain axons of ventral and dorsal RGCs, respectively. These fascicles continue their course within the tectal neuropil and around its margins. Axons leaving these fascicles branch to form arbors near their termination zone. Confocal analysis further demonstrates that fiber distribution in the neuropil is not homogeneous, suggesting that adhesion between branches of neighboring arbors produces a fine-meshed grid. Thus, *Brn3c:mGFP* labeling showed an intricate organization of axons and arbors in the wild-type tectum, which, to our knowledge, has not been the subject of previous analysis and whose functional significance is unknown.

Our screen discovered two mutants with optic tract phenotypes, clearly different from *box* and *dak* (Lee et al., 2004), and four with putative neuropil adhesion phenotypes. In *vrt* mutants, RGC axons appear diffuse and invade the tectum in several broad bundles. In *coma* mutants, the central-most fascicles are depleted of axons, and the marginal fascicles, at the dorsal and ventral edges of the optic tract, are expanded instead. Neuropil organization is also disrupted in *coma* mutants, where most axons are bundled around the margins of the neuropil and the few internal fascicles are seen meandering within the neuropil. In *bluk*, *blin* and *clew* mutants, the regularly spaced axon meshwork in the tectum is diffuse. The corresponding genes may encode adhesion molecules or factors that influence branching. For example, cadherins (Elul et al., 2003; Inoue and Sanes, 1997; Liu et al., 1999; Miskevich et al., 1998; Riehl et al., 1996; Stone and Sakaguchi, 1996; Treubert-Zimmermann et al., 2002) and immunoglobulin superfamily molecules, such as L1 and NCAM (Lyckman et al., 2000; Rathjen et al., 1987; Thanos et al., 1984; Vielmetter et al., 1991; Yamagata et al., 1995), are expressed by both RGC axons and their targets in a variety of vertebrates and could therefore underlie some of the recognition events that underlie fascicle formation, axon arbor organization or synapse stabilization.

Many areas in the vertebrate CNS are layered, and laminar targeting by axons is thought to be crucial for synaptic specificity (Sanes and Yamagata, 1999). Although a DiI tracing study in larval zebrafish made only cursory mention of tectal layers (Burrill and Easter, 1994), our confocal analysis of the *Brn3c:mGFP* and the *Shh:GFP* transgenic lines demonstrates that exactly four well-defined retinorecipient layers exist at 6 dpf. In adult teleost species, four major layers of retinal fibers have been described (Reperant and Lemire, 1976; Vanegas and Ito, 1983; von Bartheld and Meyer, 1987), with very similar characteristics to the layers we saw in the larvae. We have therefore adopted the nomenclature developed for the adult structures. Only the SFGS, receives substantial input from *Brn3c:mGFP*-expressing RGCs, and not all the axons that innervate these layers are GFP positive. Retinal axons in the SO and in the two deeper layers, SGC and SAC/SPV, are labeled in *Shh:GFP* fish and by whole-eye DiI fills, but not at all (SGC, SAC/SPV) or very little (SO) in *Brn3c:mGFP* fish. *Brn3c:mGFP* provides one of the first examples of a marker differentially expressed among RGCs with different laminar specificity.

The layer-specificity of retinal afferents is formed and maintained by molecular cues in the tectum, such as N-cadherin (Inoue and Sanes, 1997; Miskevich et al., 1998; Yamagata et al., 1995), DM-GRASP (Yamagata et al., 1995), neuropilin (Feiner et al., 1997; Takagi et al., 1995) and Ephrin B molecules (Braisted et al., 1997). Furthermore, patterning genes such *pax7* (Thompson et al., 2004) and *grg4* (Nakamura and Sugiyama, 2004) may have a role in patterning the layers of the mammalian superior colliculus. We identified an apparently novel gene, *drg*, which is important for specifying SFGS and SO layer identities. In *drg* mutants, retinal axons travel between the SO and SFGS, often in thick fascicles. The SO appears more extensively innervated. These observations suggest that axons that would normally project to the SFGS are misrouted to the SO. The *drg* gene might encode an adhesion molecule expressed in the SFGS, or a repellent factor present in the SO. Alternatively, the mutation may disrupt transduction of layer-specific cues inside retinal growth cones. The *drg* mutant is viable and therefore offers the opportunity to study the fate of the mistargeted axons in later life.

Although a great deal is known about molecules that guide axons to the tectum and align their arbors retinotopically within it, it is not clear what confines them to the tectal neuropil. In wild type, many retinal axons grow around the tectum in thick bundles, from which individual axons or small fascicles depart into the center of the neuropil. The *Brn3c:mGFP* labeling allowed us to identify three mutants, *fuzz*, *beyo* and *brek*, in which this organization has broken down. The neuropil edges are less well demarcated, and axons overshoot the borders. This description is superficially reminiscent of the zebrafish *acerebellar/fgf8* (*ace*) mutant, which lacks the midbrain-hindbrain boundary and has an enlarged tectum (Jaszai et al., 2003; Picker et al., 1999), although the phenotypes of our new mutants do not match the comparatively severe defects of *ace*. Repellent factors, such as Ephrin A3 (Hirate et al., 2001), Ephrin B2a (Wagle et al., 2004) and Tenascin (Becker et al., 2003; Perez and Halfter, 1994; Yamagata et al., 1995), as well as adhesion molecules (Demyanenko and Maness, 2003), may play a role in demarcating neuropil boundaries, so these genes represent plausible candidates for *fuzz*, *beyo* and *brek*.

Our study demonstrates the feasibility of a sensitive screen for subtle anatomical disruptions in the vertebrate brain. The genetically encoded GFP reporter provides resolution superior to carbocyanine dyes and pan-RGC markers. Our small-scale effort helped to discover larval- and adult-viable zebrafish mutants with changes in the patterning of retinotectal connections. Using *Brn3c:mGFP*, or similar lines, it should be possible to perform a saturated screen for genes assembling the optic tectum and other areas of the vertebrate brain.

We thank Pamela Raymond, Ann Wehman, Matthew Smear, and Linda Nevin for comments on the manuscript and all members of our laboratory for advice. Chi-Bin Chien (MPI Tübingen/University of Utah) provided pG1, the original GFP vector. This work was supported by a fellowship from the UCSF Neuroscience Training grant (T.X.), by the David and Lucile Packard Foundation and by grants from the NIH Eye Institute (H.B.).

Supplementary material

Supplementary material for this article is available at
http://dev.biologists.org/cgi/content/full/132/13/2955/DC1

References

Amemiya, C. T. and Zon, L. I. (1999). Generation of a zebrafish P1 artificial chromosome library. *Genomics* **58**, 211-213.

Baier, H., Klostermann, S., Trowe, T., Karlstrom, R. O., Nüsslein-Volhard, C. and Bonhoeffer, F. (1996). Genetic dissection of the retinotectal projection. *Development* **123**, 415-425.

Becker, C. G., Schweitzer, J., Feldner, J., Becker, T. and Schachner, M. (2003). Tenascin-R as a repellent guidance molecule for developing optic axons in zebrafish. *J. Neurosci.* **23**, 6232-6237.

Biederer, T., Sara, Y., Mozhayeva, M., Atasoy, D., Liu, X., Kavalali, E. T. and Sudhof, T. C. (2002). SynCAM, a synaptic adhesion molecule that drives synapse assembly. *Science* **297**, 1525-1531.

Braisted, J. E., McLaughlin, T., Wang, H. U., Friedman, G. C., Anderson, D. J. and O'Leary, D. D. (1997). Graded and lamina-specific distributions of ligands of EphB receptor tyrosine kinases in the developing retinotectal system. *Dev. Biol.* **191**, 14-28.

Burrill, J. D. and Easter, S. S., Jr (1994). Development of the retinofugal projections in the embryonic and larval zebrafish (Brachydanio rerio). *J. Comp. Neurol.* **346**, 583-600.

Culverwell, J. and Karlstrom, R. O. (2002). Making the connection: retinal axon guidance in the zebrafish. *Semin. Cell Dev. Biol.* **13**, 497-506.

DeCarvalho, A. C., Cappendijk, S. L. and Fadool, J. M. (2004). Developmental expression of the POU domain transcription factor Brn-3b (Pou4f2) in the lateral line and visual system of zebrafish. *Dev. Dyn.* **229**, 869-876.

Deiner, M. S., Kennedy, T. E., Fazeli, A., Serafini, T., Tessier-Lavigne, M. and Sretavan, D. W. (1997). Netrin-1 and DCC mediate axon guidance locally at the optic disc: loss of function leads to optic nerve hypoplasia. *Neuron* **19**, 575-589.

Demyanenko, G. P. and Maness, P. F. (2003). The L1 cell adhesion molecule is essential for topographic mapping of retinal axons. *J. Neurosci.* **23**, 530-538.

Dickson, B. J. (2002). Molecular mechanisms of axon guidance. *Science* **298**, 1959-1964.

Dingwell, K. S., Holt, C. E. and Harris, W. A. (2000). The multiple decisions made by growth cones of RGCs as they navigate from the retina to the tectum in xenopus embryos. *J. Neurobiol.* **44**, 246-259.

Drescher, U., Bonhoeffer, F. and Muller, B. K. (1997). The Eph family in retinal axon guidance. *Curr. Opin. Neurobiol.* **7**, 75-80.

D'Souza, J., Hendricks, M., Le Guyader, S., Subburaju, S., Grunewald, B., Scholich, K. and Jesuthasan, S. (2005). Formation of the retinotectal projection requires Esrom, an ortholog of PAM (protein associated with Myc). *Development* **132**, 247-256.

Easter, S. S., Jr and Nicola, G. N. (1996). The development of vision in the zebrafish (*Danio rerio*). *Dev. Biol.* **180**, 646-663.

Elul, T. M., Kimes, N. E., Kohwi, M. and Reichardt, L. F. (2003). N- and C-terminal domains of beta-catenin, respectively, are required to initiate and shape axon arbors of retinal ganglion cells in vivo. *J. Neurosci.* **23**, 6567-6575.

Erkman, L., McEvilly, R. J., Luo, L., Ryan, A. K., Hooshmand, F., O'Connell, S. M., Keithley, E. M., Rapaport, D. H., Ryan, A. F. and Rosenfeld, M. G. (1996). Role of transcription factors Brn-3.1 and Brn-3.2 in auditory and visual system development. *Nature* **381**, 603-606.

Erkman, L., Yates, P. A., McLaughlin, T., McEvilly, R. J., Whisenhunt, T., O'Connell, S. M., Krones, A. I., Kirby, M. A., Rapaport, D. H., Bermingham, J. R. et al. (2000). A POU domain transcription factor-dependent program regulates axon pathfinding in the vertebrate visual system. *Neuron* **28**, 779-792.

Feiner, L., Koppel, A. M., Kobayashi, H. and Raper, J. A. (1997). Secreted chick semaphorins bind recombinant neuropilin with similar affinities but bind different subsets of neurons in situ. *Neuron* **19**, 539-545.

Flanagan, J. G. and Vanderhaeghen, P. (1998). The ephrins and Eph receptors in neural development. *Annu. Rev. Neurosci.* **21**, 309-345.

Fricke, C., Lee, J. S., Geiger-Rudolph, S., Bonhoeffer, F. and Chien, C. B. (2001). astray, a zebrafish roundabout homolog required for retinal axon guidance. *Science* **292**, 507-510.

Higgins, D. G. and Sharp, P. M. (1988). CLUSTAL: a package for performing multiple sequence alignment on a microcomputer. *Gene* **73**, 237-244.

Hindges, R., McLaughlin, T., Genoud, N., Henkemeyer, M. and O'Leary, D. D. (2002). EphB forward signaling controls directional branch extension and arborization required for dorsal-ventral retinotopic mapping. *Neuron* **35**, 475-487.

Hirate, Y., Mieda, M., Harada, T., Yamasu, K. and Okamoto, H. (2001). Identification of *ephrin-A3* and novel genes specific to the midbrain-MHB in embryonic zebrafish by ordered differential display. *Mech. Dev.* **107**, 83-96.

Inoue, A. and Sanes, J. R. (1997). Lamina-specific connectivity in the brain: regulation by N-cadherin, neurotrophins, and glycoconjugates. *Science* **276**, 1428-1431.

Jaszai, J., Reifers, F., Picker, A., Langenberg, T. and Brand, M. (2003). Isthmus-to-midbrain transformation in the absence of midbrain-hindbrain organizer activity. *Development* **130**, 6611-6623.

Kaethner, R. J. and Stuermer, C. A. (1992). Dynamics of terminal arbor formation and target approach of retinotectal axons in living zebrafish embryos: a time-lapse study of single axons. *J. Neurosci.* **12**, 3257-3271.

Karlstrom, R. O., Trowe, T., Klostermann, S., Baier, H., Brand, M., Crawford, A. D., Grunewald, B., Haffter, P., Hoffmann, H., Meyer, S. U. et al. (1996). Zebrafish mutations affecting retinotectal axon pathfinding. *Development* **123**, 427-438.

Kay, J. N., Finger-Baier, K. C., Roeser, T., Staub, W. and Baier, H. (2001). Retinal ganglion cell genesis requires lakritz, a Zebrafish atonal Homolog. *Neuron* **30**, 725-736.

Kay, J. N., Roeser, T., Mumm, J. S., Godinho, L., Mrejeru, A., Wong, R. O. and Baier, H. (2004). Transient requirement for ganglion cells during assembly of retinal synaptic layers. *Development* **131**, 1331-1342.

Lawson, N. D., Mugford, J. W., Diamond, B. A. and Weinstein, B. M. (2003). Phospholipase C gamma-1 is required downstream of vascular endothelial growth factor during arterial development. *Genes Dev.* **17**, 1346-1351.

Lee, J. S., von der Hardt, S., Rusch, M. A., Stringer, S. E., Stickney, H. L., Talbot, W. S., Geisler, R., Nüsslein-Volhard, C., Selleck, S. B., Chien, C. B. et al. (2004). Axon sorting in the optic tract requires HSPG synthesis by *ext2* (*dackel*) and *extl3* (*boxer*). *Neuron* **44**, 947-960.

Liu, Q., Marrs, J. A. and Raymond, P. A. (1999). Spatial correspondence between R-cadherin expression domains and retinal ganglion cell axons in developing zebrafish. *J. Comp. Neurol.* **410**, 290-302.

Liu, W., Khare, S. L., Liang, X., Peters, M. A., Liu, X., Cepko, C. L. and Xiang, M. (2000). All *Brn3* genes can promote retinal ganglion cell differentiation in the chick. *Development* **127**, 3237-3247.

Liu, Y., Berndt, J., Su, F., Tawarayama, H., Shoji, W., Kuwada, J. Y. and Halloran, M. C. (2004). Semaphorin3D guides retinal axons along the dorsoventral axis of the tectum. *J. Neurosci.* **24**, 310-318.

Lyckman, A. W., Moya, K. L., Confaloni, A. and Jhaveri, S. (2000). Early postnatal expression of L1 by retinal fibers in the optic tract and synaptic targets of the Syrian hamster. *J. Comp. Neurol.* **423**, 40-51.

Mann, F., Ray, S., Harris, W. and Holt, C. (2002). Topographic mapping in dorsoventral axis of the *Xenopus* retinotectal system depends on signaling through ephrin-B ligands. *Neuron* **35**, 461-473.

McFarlane, S., Cornel, E., Amaya, E. and Holt, C. E. (1996). Inhibition of

FGF receptor activity in retinal ganglion cell axons causes errors in target recognition. *Neuron* **17**, 245-254.

McLaughlin, T., Hindges, R. and O'Leary, D. D. (2003). Regulation of axial patterning of the retina and its topographic mapping in the brain. *Curr Opin Neurobiol* **13**, 57-69.

Meek, J. (1983). Functional anatomy of the tectum mesencephali of the goldfish. An explorative analysis of the functional implications of the laminar structural organization of the tectum. *Brain Res.* **287**, 247-297.

Miskevich, F., Zhu, Y., Ranscht, B. and Sanes, J. R. (1998). Expression of multiple cadherins and catenins in the chick optic tectum. *Mol. Cell. Neurosci.* **12**, 240-255.

Mullins, M. C., Hammerschmidt, M., Haffter, P. and Nüsslein-Volhard, C. (1994). Large-scale mutagenesis in the zebrafish: in search of genes controlling development in a vertebrate. *Curr. Biol.* **4**, 189-202.

Nakamura, H. and Sugiyama, S. (2004). Polarity and laminar formation of the optic tectum in relation to retinal projection. *J. Neurobiol.* **59**, 48-56.

Neuhauss, S. C., Biehlmaier, O., Seeliger, M. W., Das, T., Kohler, K., Harris, W. A. and Baier, H. (1999). Genetic disorders of vision revealed by a behavioral screen of 400 essential loci in zebrafish. *J. Neurosci.* **19**, 8603-8615.

Neumann, C. J. and Nuesslein-Volhard, C. (2000). Patterning of the zebrafish retina by a wave of sonic hedgehog activity. *Science* **289**, 2137-2139.

Page-McCaw, P. S., Chung, S. C., Muto, A., Roeser, T., Staub, W., Finger-Baier, K. C., Korenbrot, J. I. and Baier, H. (2004). Retinal network adaptation to bright light requires tyrosinase. *Nat. Neurosci.* **7**, 1329-1336.

Perez, R. G. and Halfter, W. (1994). Tenascin protein and mRNA in the avian visual system: distribution and potential contribution to retinotectal development. *Perspect. Dev. Neurobiol.* **2**, 75-87.

Picker, A., Brennan, C., Reifers, F., Clarke, J. D., Holder, N. and Brand, M. (1999). Requirement for the zebrafish mid-hindbrain boundary in midbrain polarisation, mapping and confinement of the retinotectal projection. *Development* **126**, 2967-2978.

Rathjen, F. G., Wolff, J. M., Frank, R., Bonhoeffer, F. and Rutishauser, U. (1987). Membrane glycoproteins involved in neurite fasciculation. *J. Cell Biol.* **104**, 343-353.

Reperant, J. and Lemire, M. (1976). Retinal projections in cyprinid fishes: a degeneration and radioautographic study. *Brain Behav. Evol.* **13**, 34-57.

Riehl, R., Johnson, K., Bradley, R., Grunwald, G. B., Cornel, E., Lilienbaum, A. and Holt, C. E. (1996). Cadherin function is required for axon outgrowth in retinal ganglion cells in vivo. *Neuron* **17**, 837-848.

Roeser, T. and Baier, H. (2003). Visuomotor behaviors in larval zebrafish after GFP-guided laser ablation of the optic tectum. *J. Neurosci.* **23**, 3726-3734.

Sampath, K. and Stuart, G. W. (1996). Developmental expression of class III and IV POU domain genes in the zebrafish. *Biochem. Biophys. Res. Commun.* **219**, 565-571.

Sanes, J. R. and Yamagata, M. (1999). Formation of lamina-specific synaptic connections. *Curr. Opin. Neurobiol.* **9**, 79-87.

Serafini, T. (1999). Finding a partner in a crowd: neuronal diversity and synaptogenesis. *Cell* **98**, 133-136.

Stone, K. E. and Sakaguchi, D. S. (1996). Perturbation of the developing *Xenopus* retinotectal projection following injections of antibodies against beta1 integrin receptors and N-cadherin. *Dev. Biol.* **180**, 297-310.

Stuermer, C. A. (1988). Retinotopic organization of the developing retinotectal projection in the zebrafish embryo. *J. Neurosci.* **8**, 4513-4530.

Takagi, S., Kasuya, Y., Shimizu, M., Matsuura, T., Tsuboi, M., Kawakami, A. and Fujisawa, H. (1995). Expression of a cell adhesion molecule, neuropilin, in the developing chick nervous system. *Dev. Biol.* **170**, 207-222.

Thanos, S., Bonhoeffer, F. and Rutishauser, U. (1984). Fiber-fiber interaction and tectal cues influence the development of the chicken retinotectal projection. *Proc. Natl. Acad. Sci. USA* **81**, 1906-1910.

Thompson, J., Lovicu, F. and Ziman, M. (2004). The role of Pax7 in determining the cytoarchitecture of the superior colliculus. *Dev. Growth Differ.* **46**, 213-218.

Treubert-Zimmermann, U., Heyers, D. and Redies, C. (2002). Targeting axons to specific fiber tracts in vivo by altering cadherin expression. *J. Neurosci.* **22**, 7617-7626.

Trowe, T., Klostermann, S., Baier, H., Granato, M., Crawford, A. D., Grunewald, B., Hoffmann, H., Karlstrom, R. O., Meyer, S. U., Muller, B. et al. (1996). Mutations disrupting the ordering and topographic mapping of axons in the retinotectal projection of the zebrafish, *Danio rerio*. *Development* **123**, 439-450.

van Eeden, F. J., Granato, M., Odenthal, J. and Haffter, P. (1999). Developmental mutant screens in the zebrafish. *Methods Cell Biol.* **60**, 21-41.

Vanegas, H. and Ito, H. (1983). Morphological aspects of the teleostean visual system: a review. *Brain Res.* **287**, 117-137.

Vielmetter, J., Lottspeich, F. and Stuermer, C. A. (1991). The monoclonal antibody E587 recognizes growing (new and regenerating) retinal axons in the goldfish retinotectal pathway. *J. Neurosci.* **11**, 3581-3593.

von Bartheld, C. S. and Meyer, D. L. (1987). Comparative neurology of the optic tectum in ray-finned fishes: patterns of lamination formed by retinotectal projections. *Brain Res.* **420**, 277-288.

Wagle, M., Grunewald, B., Subburaju, S., Barzaghi, C., Le Guyader, S., Chan, J. and Jesuthasan, S. (2004). EphrinB2a in the zebrafish retinotectal system. *J. Neurobiol.* **59**, 57-65.

Walz, A., McFarlane, S., Brickman, Y. G., Nurcombe, V., Bartlett, P. F. and Holt, C. E. (1997). Essential role of heparan sulfates in axon navigation and targeting in the developing visual system. *Development* **124**, 2421-2430.

Wang, S. W., Mu, X., Bowers, W. J., Kim, D. S., Plas, D. J., Crair, M. C., Federoff, H. J., Gan, L. and Klein, W. H. (2002). Brn3b/Brn3c double knockout mice reveal an unsuspected role for Brn3c in retinal ganglion cell axon outgrowth. *Development* **129**, 467-477.

Xiang, M., Zhou, L., Macke, J. P., Yoshioka, T., Hendry, S. H., Eddy, R. L., Shows, T. B. and Nathans, J. (1995). The Brn-3 family of POU-domain factors: primary structure, binding specificity, and expression in subsets of retinal ganglion cells and somatosensory neurons. *J. Neurosci.* **15**, 4762-4785.

Yamagata, M., Herman, J. P. and Sanes, J. R. (1995). Lamina-specific expression of adhesion molecules in developing chick optic tectum. *J. Neurosci.* **15**, 4556-4571.

Yamagata, M., Weiner, J. A. and Sanes, J. R. (2002). Sidekicks: synaptic adhesion molecules that promote lamina-specific connectivity in the retina. *Cell* **110**, 649-660.

Zuber, M. X., Strittmatter, S. M. and Fishman, M. C. (1989). A membrane-targeting signal in the amino terminus of the neuronal protein GAP-43. *Nature* **341**, 345-348.